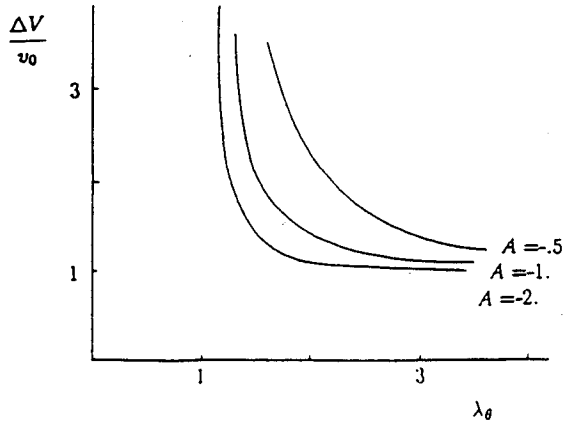

Fig. 3 Energy cost for different initial conditions.

Also, the total energy expenditure required for rendezvous is

$$\Delta V = \int_0^T |a_c| \, dt = v_0 \sqrt{1 + \frac{1}{\frac{A^2}{1+A^2}\lambda^2 - 1}} \qquad (11)$$

where v_0 ($= \sqrt{\dot{r}_0^2 + r_0^2\dot{\theta}_0^2}$) is the magnitude of initial relative velocity. The ΔV required for exoatmospheric rendezvous is proportional to and always greater than the initial relative velocity. For a smaller value of $|A|$ or λ, a larger energy cost is required, as depicted in Fig. 3.

III. Conclusion

In this rendezvous guidance, the magnitude of the commanded acceleration is programmed similarly to that of modified true proportional navigation, but it is applied with a bias angle to the direction normal to LOS in general. Under this guidance scheme, the closed-form solution of the relative motion described in a polar coordinate can be simply obtained as a function of range-to-go or LOS angle. The relative rendezvous path is a form of spiral function, which means that the direction of the relative velocity is unchanged relative to the LOS, and the total commanded acceleration is always applied in a fixed direction related to the relative velocity during the course of the rendezvous. Also, the energy expenditure required is proportional to and greater than the initial magnitude of relative velocity.

References

[1]Guelman, M., "A Qualitative Study of Proportional Navigation," *IEEE Transactions on Aerospace and Electronic Systems*, Vol. AES-7, No. 4, 1971, pp. 337-343.

[2]Guelman, M., "Proportional Navigation with a Maneuvering Target," *IEEE Transactions on Aerospace and Electronic Systems*, Vol. AES-8, No. 3, 1972, pp. 364-371.

[3]Guelman, M., "Missile Acceleration in Proportional Navigation," *IEEE Transactions on Aerospace and Electronic Systems*, Vol. AES-9, No. 3, 1973, pp. 462-463.

[4]Becker, K., "Closed-Form Solution of Pure Proportional Navigation," *IEEE Transactions on Aerospace and Electronic Systems*, AES-26, No. 3, 1990, pp. 526-533.

[5]Murtaugh, S. A., and Criel, H. E., "Fundamentals of Proportional Navigation," *IEEE Spectrum*, Vol. 3, No. 6, 1966, pp.75-85.

[6]Guelman, M., "The Closed-Form Solution of True Proportional Navigation," *IEEE Transactions on Aerospace and Electronic Systems*, AES-12, No. 4, 1976, pp. 472-482.

[7]Cochran, J. E., Jr., No, T. S., and Thaxton, D. G., "Analytical Solutions to a Guidance Problem," *Journal of Guidance, Control, and Dynamics*, Vol. 14, No. 1, 1991, pp. 117-122.

[8]Yuan, P. J., and Chern, J. S., "Solutions of True Proportional Navigation for Maneuvering and Non-maneuvering Targets," *Journal of Guidance, Control, and Dynamics*, Vol. 15, No. 1, 1992, pp. 268-271.

[9]Yang, C. D., Yeh, F. B., and Chen, J. H., "The Closed-Form Solution of Generalized Proportional Navigation," *Journal of Guidance, Control, and Dynamics*, Vol. 10, No. 2, 1987, pp. 216-218.

[10]Yang, C. D., Hsiao, F. B., and Yeh, F. B., "Generalized Guidance Law for Homing Missiles," *IEEE Transactions on Aerospace and Electronic Systems*, Vol. 25, No. 2, 1989, pp. 197-212.

[11]Yuan, P. J., and Hsu, S. C., "Exact Closed-Form Solution of Generalized Proportional Navigation," *Journal of Guidance, Control, and Dynamics*, Vol. 16, No. 5, 1993, pp. 963-966.

[12]Yuan, P. J., and Chern, J. S., "Ideal Proportional Navigation," *Journal of Guidance, Control, and Dynamics*, Vol. 15, No. 5, 1992, pp. 1161-1165.

[13]Yuan, P. J., and Chern, J. S., "Analytic Study of Biased Proportional Navigation," *Journal of Guidance, Control, and Dynamics*, Vol. 15, No. 1, 1992, pp. 185-190.

[14]Guelman, M., "Guidance for Asteroid Rendezvous," *Journal of Guidance, Control, and Dynamics*, Vol. 14, No. 5, 1991, pp. 1080-1083.

[15]Jensen, D. L., "Kinematics of Rendezvous Maneuvers," *Journal of Guidance, Control, and Dynamics*, Vol. 7, No. 3, 1984, pp. 307-314.

[16]Niemi, N. J., "Investigation of a Terminal Guidance System for a Satellite Rendezvous," *AIAA Journal*, Vol. 1, No. 2, 1963, pp. 405-411.

[17]Cicolani, L. S., "Trajectory Control in Rendezvous Problems Using Proportional Navigation," NASA TN-D-772, April 1961.

[18]Steffan, K. F., "Satellite Rendezvous Terminal Guidance System," *American Rocket Society Journal*, Vol. 31, No. 11, 1961, pp. 1516-1521.

Elastoplastic Analysis and Cumulative Damage Study of a Lanyard Under Dynamic Conditions

B. S. Nataraju* and B. P. Nagaraj†
ISRO Satellite Centre, Bangalore 560 017, India

Introduction

THE coilable lattice boom (CLB) shown in Fig. 1a is used to deploy a solar sail. Figure 1b shows the sail stowed against the deck of the satellite and held by six launch restraint rods. One end of each launch restraint rod is attached to the spider block and the other end to the hold down assembly. Figure 1c shows the pop-out spring, housed inside the spider block. The CLB is stowed inside a canister with a preloaded tip plate. A lanyard made of thin beryllium-copper strip is wound on a motor-driven pulley with one end attached to the tip plate. The rate of deployment of the CLB is controlled by the lanyard. In the stowed configuration the lanyard is slack. When the tie rod is cut by a pyrocutter, the whole system jumps freely through 0.02 m and then the lanyard becomes taut.

The CLB has a large strain energy stored due to the coiling of elements. The spider block with pop-out spring, the launch restraint rods, and the tip plate possess large strain energy. This energy is absorbed by the lanyard after the system is released.

This Note addresses the formulation of equations of motion for this system to assess the deformation and the load acting on the lanyard. An elastoplastic analysis is necessary as the lanyard is yielding after first release. The system will be stowed back and released for different test configurations before launch. The lanyard undergoes a permanent deformation after each release. Hence, the cumulative damage at the end of each release is calculated. Furthermore, the number of cycles the lanyard would withstand before failure is assessed to ensure that the lanyard is intact during the on-orbit deployment.

Received Aug. 12, 1991; revision received Dec. 1, 1992; accepted for publication Dec. 23, 1992. Copyright © 1993 by the American Institute of Aeronautics and Astronautics, Inc. All rights reserved.

*Head, Dynamics and Analysis Section, Spacecraft Mechanisms Division.

†Engineer, Spacecraft Mechanisms Division.

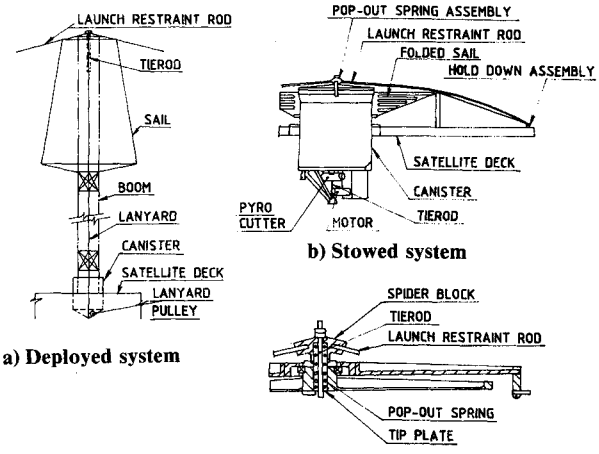

Fig. 1 Deployed and stowed configuration of the boom and sail assembly.

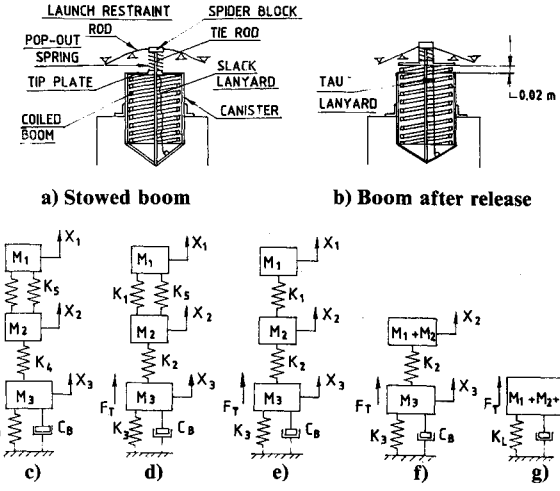

Fig. 2 Schematic representation of the stowed and released system with idealized spring mass system.

Mathematical Modeling

The stowed and released configuration of the deployment mechanism is shown in Fig. 2a. The physical parameters are presented in Table 1. This is modeled as a three-degree-of-freedom (DOF) system as shown in Fig. 2c. The equations of motion for this system are derived by using Lagrange's equation[1]:

$$M_1\ddot{X}_1 + K_1(X_1 - X_2) + K_5(X_1 - X_2) = K_1 D_P + K_5 D_L \quad (1)$$

$$M_2\ddot{X}_2 + K_1(X_2 - X_1) + K_5(X_2 - X_1) + K_2(X_2 - X_3) + K_4(X_2 - X_3) + K_1 D_P + K_5 D_L = K_4 D_T \quad (2)$$

$$M_3\ddot{X}_3 + K_2(X_3 - X_2) + K_3 X_3 + K_4(X_3 - X_2) + C_B\dot{X}_3 + K_4 D_T = F_T \quad (3)$$

where X_i and $\dot{X}_i$ are the displacement and velocity of mass M_i, respectively, and

$$C_B = \xi 2\sqrt{K_3 M_3}$$

where ξ is the damping ratio.

These equations are modified depending on the instantaneous status of each individual system. The tip plate, which is simply supported on a canister shell with a preload of 980 N, attains free-free conditions[2] when it moves through 0.0015 m as shown in Fig. 2d. The constraints are

$$K_2 = 0 \text{ and } K_4 = 653{,}334 \text{ N/m for } (X_2 - X_3) < 0.0015 \text{ m} \quad (4)$$

$$K_4 = 0 \text{ and } K_2 = 211{,}097 \text{ N/m for } (X_2 - X_3) \geq 0.0015 \text{ m} \quad (5)$$

The CLB exhibits two stiffness characteristics given by

$$K_3 = 7500 \text{ N/m} \quad \text{for} \quad X_3 < 0.003 \text{ m} \quad (6)$$

$$K_3 = 187.5 \text{ N/m} \quad \text{for} \quad X_3 \geq 0.003 \text{ m} \quad (7)$$

The launch restraint rods become free when mass M_1 moves through 0.0435 m as shown in Fig. 2e. The pop-out spring locks with the tip plate when M_1 moves through 0.07 m. The constraints are

$$K_5 = 0 \quad \text{and} \quad D_L = 0 \quad \text{for} \quad (X_1 - X_2) \geq 0.0435 \text{ m} \quad (8)$$

$$K_1 = 0 \quad \text{and} \quad D_P = 0 \quad \text{for} \quad (X_1 - X_2) \geq 0.070 \text{ m} \quad (9)$$

At this stage the system behaves as a two DOF system as shown in Fig. 2f. The differential equations along with the preceding constraints are solved by fourth-order Runge-Kutta method with the following initial conditions.

At time $t = 0$,

$$X_i = 0 \quad \text{and} \quad \dot{X}_i = 0 \quad (10)$$

for $i = 1$ to 3.

From this, the time taken and the velocity of the system at a jump distance of 0.02 m is calculated. After the jump distance of 0.02 m, the slack lanyard becomes taut. The system now behaves as a single DOF system as shown in Fig. 2g. The equation of motion for this is given by

$$M_4\ddot{X}_4 + f(X_4, P) + C_B\dot{X}_4 = F_T \quad (11)$$

At $t = 0$,

$$X_4 = 0 \quad \text{and} \quad \dot{X}_4 = \dot{X}_3 \text{ (at 0.02 m)} \quad (12)$$

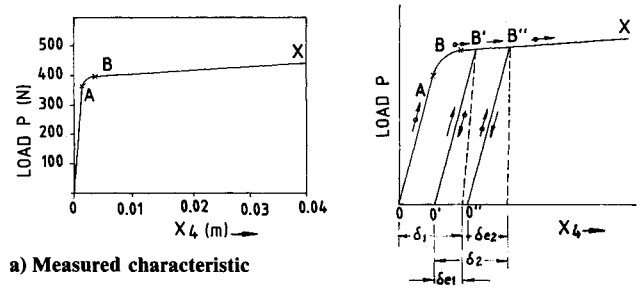

a) Measured characteristic

b) Schematic of repeated loading X_4 deformation of lanyard

Fig. 3 Force-deflection characteristics of the lanyard.

Table 1 Physical parameters of the system

D_L	Initial deflection of launch restraint rods	0.0435 m
D_P	Initial compression of pop-out spring	0.088 m
D_T	Initial deflection of tip plate	0.0015 m
F_T	Force due to compression of boom coils	35.0 N
K_1	Stiffness of pop-out spring	191.295 N/m
K_5	Stiffness of launch restraint rods	1340.0 N/m
M_1	Mass of launch restraint rods and spider block	0.203 kg
M_2	Mass of tip plate	0.48 kg
M_3	Mass of boom coils	3.42 kg

where $M_4 = M_1 + M_2 + M_3$ as all masses get attached to the lanyard, and $f(X_4, P)$ is a force-deflection function of the lanyard fitted for measured force-deflection characteristics of Fig. 3a.

1) For the linear portion of the curve OA: $X_4 \leq 0.001516$ m

$$f(X_4, P) = K_L X_4 \tag{13}$$

where $K_L = 236{,}000$ N/m.

2) For the nonlinear portion of curve[3] AB: $0.001516 \text{ m} < X_4 < 0.004064$ m

$$f(X_4, P) = kX_4^r \tag{14}$$

where $k = 744.418$ and $r = 0.1128$.

3) For the linear portion of curve BC: $X_4 \geq 0.004064$ m

$$f(X_4, P) = AX_4 + B \tag{15}$$

where $A = 2459.4$ and $B = 390.0$.

The differential equation (11), along with Eqs. (13-15), is solved for the deformation and shock load on the lanyard.

The system is released several times for different test configurations before launch. To calculate the cumulative deformation at the end of each test Fig. 3b is used. Referring to Fig. 3b, the force-deflection characteristic of the lanyard for repeated loading is measured on a tensile testing machine. The curve shows a linear relationship approximately parallel to OA for the second and subsequent loading of the lanyard. Hence, a linear relationship $O'B'$ and $O''B''$, etc., is assumed for calculation. The first cycle refers to the curve $OAB'O'$. The second cycle is $O'B'B''O''$ and so on.

The deformation of the lanyard is calculated for the first release by using the curve $OABX$. For the second release, the deformation of the lanyard is calculated by using the curve $O'B'X$. δ_1 and δ_2 are the deformations including the elastic limit for the first and second releases, respectively. For the third release, curve $O''B''X$ is used. This is extended for subsequent releases. δe_1 and δe_2 are the elastic deformations at the end of each release. Therefore, for the nth release for which failure occurs, the cumulative deformation is given by

$$(\delta_1 + \delta_2 + \cdots + \delta_n) - (\delta e_1 + \delta e_2 + \cdots + \delta e_{n-1}) > \delta u \tag{16}$$

where δu is the total elongation of the lanyard before failure. Hence, n is the number of cycles the lanyard can withstand before failure.

The energy due to the subsystems at the end of 0.02-m jump distance is absorbed by the lanyard. The area under the curve OAB' and $O'B'B''$ is the energy absorbed for the first and second releases, respectively. This energy is much higher than the energy in the elastic region of the force-deflection curve. Hence, the lanyard undergoes plastic deformation for each release. The force increase for each release is due to the positive slope of the force-deflection curve.

Results and Discussions

Figure 4 shows the results of the analytical equations for 0 and 20% damping. The peak point on Fig. 4a shows the lanyard deformation. The velocity of the system drops down when the lanyard becomes active and will be zero when the deformation is maximum. The inertial force of the system for this deformation, shown in Fig. 4c, is the peak load acting on the lanyard. The magnitude of the inertial force is large before the 0.02-m jump distance. This load, however, does not affect the slack lanyard. This dynamic load acting on the lanyard is significant when the system reaches the jump distance of 0.02 m. The maximum deformation is 0.005367 m for zero damping, exceeding the elastic deformation of 0.001516 m. This shows that the lanyard has plastically deformed.

This deformation of the lanyard corresponds to zero damping. But the damping present at the hinges of the boom, between boom coils and in the sail, reduces this deformation.

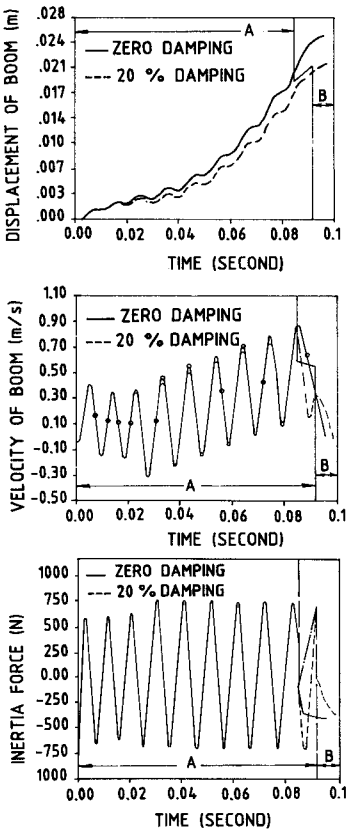

Fig. 4 Displacement, velocity, and inertial force response of the boom and lanyard for 0 and 20% damping: A = slack lanyard region and B = taut lanyard region.

The lanyard is assumed to be held rigid, but the same is wound on a pulley. Hence, some shock load is absorbed by the shaft of the pulley.

By using the preceding mathematical model for repeated releases, with no change in test configuration for a jump distance of 0.02 m, the lanyard can withstand 12 cycles. Because of the strain hardening, the total elongation for repeated loading is marginally less compared to single loading until failure. Hence, the lanyard can withstand marginally less than 12 cycles.

In this analysis, the cycles are calculated based on the energy-absorbing capacity of the lanyard. Hence, the material can withstand a low number of cycles. This is not a low-cycle fatigue phenomenon where the load is kept constant for each cycle without energy considerations. The plastic deformation for the second and subsequent cycles is negligibly small. Hence, in low-cycle fatigue the material can withstand a large number of cycles.

In this Note, the static force-deflection characteristic of the lanyard is used. The material characteristics for the beryllium-copper strip at high strain rates are difficult to determine. The exact strain rate the lanyard undergoes is not known. The material behavior will be different for different strain rates.

The system undergoes tests in different configurations on the ground before launch, by detaching subsystems like the sail assembly and removing the preload on the tip plate. The cumulative deformation at the end of all test configurations is calculated. This should be far less than the total elongation of the lanyard before failure.

Testing the whole system is expensive; hence, a test has been carried out as described in the Appendix. The mathematical model has been assessed with regard to the behavior of the lanyard.

Conclusions

This Note has described the dynamic load coming on the lanyard due to the energies of various subsystems of the CLB

and the sail assembly. Practical aspects of mathematical modeling and simulation have ben emphasized. This Note presents a picture of elastoplastic behavior of the lanyard under different test conditions. A mathematical approach has been developed for studying cumulative deformation and assessing the margin of safety in terms of number of cycles before failure.

Appendix: Ground Simulation Model

The system under consideration is a CLB with no preload on the tip plate, without pop-out spring and sail assembly. This is released under gravity for a jump distance of 0.023 m with the lanyard becoming taut, when the system reaches this jump distance. Then the system is retracted and adjusted such that the slack lanyard will be taut for a jump distance of 0.043 m, when the system is released. The system is retracted and the preceding procedure is repeated for the jump distances of 0.063 m, in steps of 0.01 m, until the lanyard fails. In the test, the lanyard failed for the 0.113-m jump distance with all cumulative damages due to earlier tests.

The mathematical model developed for this configuration is a single DOF system with bilinear boom stiffness characteristics. The deformation of the lanyard is calculated based on the force-deflection characteristics. The cumulative permanent deformation of the lanyard calculated by this model exceeded the allowable deformation for the jump distance of 0.103 m indicating lanyard failure. This is in agreement with test results which showed the failure for a jump distance of 0.113 m.

Acknowledgments

The authors thank M. N. Sathyanarayan, Head, and M. Nageswara Rao, Deputy Head, Spacecraft Mechanisms Division for their encouragement and useful discussions. The authors thank N. C. Bhat, Head, Design and Development Section, and T. P. Murali for useful suggestions. The authors thank V. Sridharamurthy and K. S. Balan for providing the technical data. They thank A. V. Patki, Director, Mechanical Systems Group, and K. Kasturirangan, Director, ISRO Satellite Centre, for their encouragement.

References

[1]Tse, F. S., Morse, I. E., and Hinkle, R. T., "The Lagrange Equation," *Mechanical Vibration,* Prentice-Hall, India, 1968, pp. 159–170.

[2]Leissa, A. M., "Vibration of Plates," NASA SP-160, 1969.

[3]Marin, J., "Nominal Stress-Strain Properties in Simple Tension," *Mechanical Behavior of Engineering Materials,* Prentice-Hall, India, 1966, pp. 6–11.

Solutions to Parameter Optimal Control

Yiyuan Zhao*
University of Minnesota, Minneapolis, Minnesota 55455

Introduction

PARAMETER optimal control optimizes parameters subject to differential constraints. It is between regular optimal control and parameter optimization. It has many applications. In particular, trajectory optimization problems can be converted into parameter optimal control with various control parameterizations.

Some work has been done on parameter optimal control. Vincent and Grantham[1] studied necessary conditions using a parameter optimization method. Stengel[2] discussed possible applications of the problem. Rogers[3] developed a first-order numerical method.

This Note uses two approaches and derives the first- and second-order conditions for unconstrained parameter optimal control. The obtained gradient expressions can be used effectively in numerical solutions.

Received Aug. 8, 1992; revision received Feb. 28, 1993; accepted for publication May 10, 1993. Copyright © 1993 by Y. Zhao. Published by the American Institute of Aeronautics and Astronautics, Inc., with permission.

*Assistant Professor, Department of Aerospace Engineering and Mechanics. Member AIAA.

Problem Statement

A parameter optimal control problem seeks to minimize

$$I = \phi(x_f, \pi) + \int_{t_0}^{t_f} L(t, x, \pi)\, dt \tag{1}$$

subject to

$$\dot{x} = f(t, x, \pi) \tag{2}$$

where $x(t)$ is an $n \times 1$ state vector, π is a $p \times 1$ parameter vector, and both ϕ and L are scalars. We assume that t_0 and t_f are fixed, and $x(t_0) = x_0$ is specified. π is constant over $[t_0, t_f]$.

Parameter optimal control problems appear naturally in engineering. Engine parameter optimizations, for example, are subject to motion dynamics. A trajectory optimization problem can be solved efficiently with parameter optimal control. Parameter optimal control can also be used to determine feedback gains in a nonlinear system. In these applications, the gradient expressions derived in this Note require many fewer numerical integrations than a direct digital differentiation.

Solution Methods: Overview

There are two basic approaches to solve a parameter optimal control problem. Parameter optimal control can be viewed as a special optimal control problem that only uses parameters. Also, it can be seen as a special parameter optimization problem with differential constraints. These two interpretations provide two basic solution methods.

In the optimal control approach, the differential constraints are adjoined to the performance index through the use of Lagrange multiplier functions. As a result, one obtains simple expressions for both the first- and second-order gradients. The parameter optimization approach produces consistent results but does not lead to clean expressions for the second-order gradient.

One can combine the two approaches in constructing numerical methods. Nonlinear programming algorithms can be used directly with the simple expressions of the first- and second-order gradients from the optimal control approach.

Necessary Conditions

In the optimal control approach, we adjoin Eq. (2) into the performance index I in Eq. (1). The augmented cost functional is

$$J = \phi(x_f, \pi) + \int_{t_0}^{t_f} \left[H(t, x, \pi, \lambda) - \lambda^T \dot{x}\right] dt \tag{3}$$

where $\lambda(t)$ is an $n \times 1$ Lagrange multiplier function, and H is the Hamiltonian defined as

$$H(t, x, \pi, \lambda) \triangleq L(t, x, \pi) + \lambda^T f(t, x, \pi) \tag{4}$$

The first variation of J is

$$\begin{aligned}\delta J &= \phi_{x_f}\delta x_f + \phi_\pi \delta\pi \\ &\quad + \int_{t_0}^{t_f} \left[H_x \delta x + H_\pi \delta\pi - \lambda^T \delta\dot{x} + \delta\lambda^T (f - \dot{x})\right] dt \\ &= (\phi_{x_f} - \lambda_f^T)\delta x_f + \lambda_0^T \delta x_0 \\ &\quad + \left[\phi_\pi + \int_{t_0}^{t_f} H_\pi\, dt\right]\delta\pi + \int_{t_0}^{t_f} (H_x + \dot{\lambda}^T)\delta x\, dt \end{aligned} \tag{5}$$

Noting $\delta x_0 = 0$ and choosing

$$\dot{\lambda} = -H_x^T \qquad \lambda(t_f) = \phi_{x_f}^T \tag{6}$$